


INVESTIGATION OF ELECTROMAGNETIC AND MECHANICAL STIRRING SEQUENCE EFFECTS ON PRODUCTION OF MAGNESIUM MATRIX NANOCOMPOSITE

A. H. Jabbari and M. Sedighi 

School of Mechanical Engineering, Iran University of Science and Technology, Narmak, Tehran 1684613114, Iran

Copyright © 2019 American Foundry Society
<https://doi.org/10.1007/s40962-019-00374-5>

Abstract

In this article, mechanical and electromagnetic stirring methods were employed in different sequences during the stir casting process in order to fabricate metal matrix nanocomposite. Sequence of stirring methods can affect particle distribution and porosity of the composite and consequently alter microstructural and mechanical properties. To investigate the stirring effects, AZ31B/1.5 vol% nano- Al_2O_3 composites were produced using different stirring processes. Next, the as-cast billets were hot-extruded at 350 °C using 20:1 extrusion ratio. The results showed that the sequence of the mechanical and electromagnetic stirring methods have considerable effects on porosity, grain size, microhardness, tensile properties, and high cycle fatigue behavior of the composites. The best mechanical and microstructural properties were obtained

by the mechanical stirring method followed by the electromagnetic stirring. The samples produced by this method exhibited 44.7% decrease in grain size, 40.8% increase in hardness, 12.3% enhancement in ultimate tensile strength, and 16.5% improvement in maximum elongation, compared to the monolithic AZ31B sample. Additionally, the endurance limit of the composite enhanced about 21% in high cycle fatigue regime. On the other hand, nanocomposite fabricated by mechanical stirring method showed the poorest behavior under cyclic loading.

Keywords: magnesium, metal matrix composite, stir casting, mechanical stirring, electromagnetic stirring, high cycle fatigue

Introduction

Nowadays, weight reduction in the transportation and other related industries has become a major challenge to face costs and environmental issues. Among the structural metals, magnesium (Mg) is a reasonable choice as the lightest one. Moreover, it possesses high specific strength, excellent machinability, and preferable damping capacity.¹⁻⁷ Nonetheless, magnesium and its alloys have some undesirable mechanical and metallurgical properties such as poor wear, corrosion, and creep resistance. Consequently, their industrial applications are limited.⁸⁻¹⁴ As a solution, producing metal matrix composites (MMCs) with magnesium matrix phase has been considered during recent decades.¹⁵⁻¹⁷

There are several methods to produce MMCs. Among them, stir casting is one of the most applicable methods for fabrication of discontinuous metal matrix composites because of its low processing costs and rapid production procedure.¹⁸ Stirring molten metal can be performed using

different stirring techniques. The most common stirring technique is to utilize a rotating mechanical impeller, which creates shear stress in the melt and distributes the reinforcing particles.^{17,19-21} On the other hand, it could make unwanted pores, gas bubbles, and impurities in the molten metal. Besides, mechanical stirring might not be sufficient to break all the agglomerations of reinforcing particles, especially in the case of nano-sized particles.

Electromagnetic stirring (created by targeted electromagnetic coils) is another stirring method during the stir casting process. It may be effective for producing a desirable MMC by helping to distribute the reinforcing particles as well as decreasing the dendritic structures and refining the grains during solidification.^{22,23} Indeed, most magnesium alloys have a large solidification range, leading to formation of microshrinkage and dendritic structures.²⁴ Dendritic structures and coarse grains could push the reinforcing particles during solidification step and cause an undesirable redistribution of them, resulting in formation of particle agglomerations. As a solution, applying electromagnetic

stirring up to the solidification step could reduce the detrimental effects of this phenomenon.^{25,26} This type of stirring prevents the distributed particles to float or settle during the solidification. Furthermore, electromagnetic stirring could help to produce a defect-free composite, reducing segregation and internal cracks. Electromagnetic stirring exerts a body force to the molten metal. By applying this stirring technique during the cooling step, the trapped gas bubbles and considerable particle agglomerations could be floated or settled. This would result in less unwanted porosity and better distribution of the reinforcing particles. Nevertheless, using the electromagnetic stirrer individually cannot efficiently distribute the reinforcements, since it just exerts a body force. Thus, applying both mechanical and electromagnetic stirring techniques might be beneficial. In fact, combining both shear and body forces could cause more turbulence in the molten metal and may benefit from the advantages of each stirring method. However, the sequence and the direction of the stirring are vital to be investigated.

Fatigue behavior of Mg-based MMCs is also a key parameter in load-bearing applications. In the literature, authors mostly have studied the effects of different reinforcement types, the particle size, and the particle volume fraction on the overall mechanical and fatigue behavior of magnesium matrix composites. Vaidya et al.²⁷ studied the effects of particle size and volume fraction of micro-sized SiC particles on AZ91/SiC composite. Squeeze casting and hot extrusion methods were applied to fabricate the composite. To mix the molten matrix and the SiC particles before casting, a mechanical impeller was used. While adding 15- μm SiC particles to AZ91D matrix led to an improvement in high cycle fatigue behavior, the composites containing 52- μm SiC particles exhibited a reduced fatigue life (compared to the monolithic AZ91D). It was reported that the presence of bigger reinforcing particles could result in a decrease in crack initiation and/or crack growth resistance. Moreover, a larger percentage of the cracked particles was observed on the fracture surface of the composites containing 52- μm SiC particles. Goh et al.^{28,29} evaluated the effects of Y_2O_3 and CNT nanoparticles on fatigue behavior of Mg matrix composite under cyclic loading with constant stress amplitudes. The composites were fabricated by disintegrated melt deposition technique (DMD). During this technique, the mixture of the molten magnesium and the reinforcing particles was stirred mechanically. The obtained ingots were hot-extruded at 350 °C. The results of the plastic strain amplitude versus the number of cycles to failure showed that the cycles to failure for the Mg/ Y_2O_3 nanocomposites and the monolithic Mg are comparable. In the matrix of the composite and near the particles, localized plastic deformation occurred due to the considerable difference between elastic moduli of the two phases. In addition, this plastic deformation caused a triaxial stress state and stress gradients around the reinforcing phase. As a result, compared to the

monolithic magnesium, the composite could not show a superior behavior. For Mg/CNT nanocomposite, the number of cycles to failure was lower than that for pure Mg samples. The presence of voids at the nanocomposite specimen surface (where the clusters of CNTs were found) was considered as the main reason for this degradation.

Srivatsan et al.³⁰ devoted their effort to observing the fatigue behavior of AZ31/ Al_2O_3 nanocomposite fabricated by DMD technique and hot extrusion process. The results revealed that the cyclic fatigue resistance of the nanoparticle-reinforced composite improved over the entire range of the maximum stress. The desirable influence of the nano-sized reinforcing particles in delaying crack initiation and retarding crack propagation through the matrix was reported as the improvement reasons. Also, Hassan et al.³¹ evaluated the effects of SiC particle volume fraction on high cycle fatigue behavior of AZ91/SiC composite prepared by squeeze casting and hot extrusion. According to the results, increasing the SiC particle content degraded the strain-controlled fatigue properties in the low cycle fatigue, while it could increase the fatigue life in high cycle regime. Indeed, composite with higher SiC content exhibited increased cyclic stress amplitudes for a given cyclic strain amplitude. In addition, increasing the SiC volume fraction could yield highly localized plastic strain in the magnesium matrix.

In general, distribution of nano-sized reinforcing particles in metal matrix is a challenging procedure requiring special equipment (such as ultrasonic probe which is expensive, and usually, its energy is localized in a small region underneath the probe³²) or high amounts of energy (for semisolid stirring). Thus, these kinds of procedures usually cannot be applied for mass production. In this study, the main concern is to propose a new simple method by evaluating the combination of electromagnetic and mechanical stirring in order to produce magnesium matrix nanocomposites. Although this combination might have some advantages, the sequence of stirring methods could alter both particle distribution and porosity percentage of the fabricated composites and consequently influence microstructural and mechanical properties. Thus, the microstructural and mechanical properties of the samples with different stirring processes were evaluated including grain size, microhardness, tensile test, and high cycle fatigue behavior.

Experimental Details

Materials

To fabricate AZ31B/1.5 vol% nano- Al_2O_3 composite, AZ31B ingot (3.05%Al, 0.97 wt%Zn, 0.37 wt%Mn, 0.0018 wt%Fe, 0.041 wt%Si, 0.023 wt%Cu, and 0.0003 wt%Ni and balance Mg) supplied from Hunan High

Broad New Material was used. Also, nano- Al_2O_3 particles (average diameter of 50 nm) were employed as the reinforcing phase.

Producing Metal Matrix Nanocomposite

According to Figure 1, the AZ31B ingot was drilled (25 holes with a diameter of 6 mm and a depth of 50 mm) and washed by acetone in order to remove the existing contaminations. Next, the holes were filled precisely with nano- Al_2O_3 particles. The weight fractions of the AZ31B and Al_2O_3 particles were measured accurately to produce AZ31B/1.5 vol% Al_2O_3 nanocomposite. Before filling the holes, nano-sized Al_2O_3 particles were dispersed for 20 min using an ultrasonic tank (with an ultrasonic frequency of 28 kHz) to break the particle agglomerations.

In order to implement the stir casting process, first, the main chamber of the stir casting apparatus was vacuumed and then filled with high-purity argon gas (99.9995%) to protect AZ31B from burning during the process. Then, the temperature was increased up to 780 °C using electrical resistance heating elements around the chamber. When the AZ31B ingot was melted completely, the first step of the stirring process was performed and continued for 10 min. The second stirring step for the electromagnetic stirring took place from 780 until 650 °C, with a cooling rate of 8 °C/min. Next, the chamber was pulled out from the furnace and cooled in the air. An additional experiment, where ingots of AZ31B without reinforcing particles were produced, acted as a baseline in comparison with the

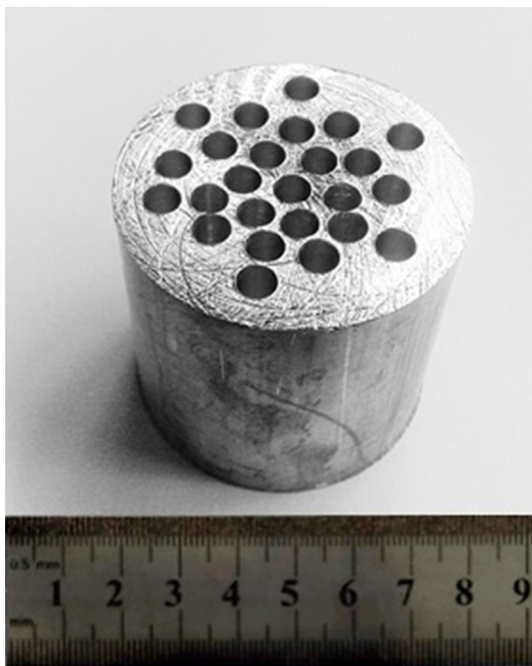


Figure 1. Initial drilled ingot of AZ31B, before filling with Al_2O_3 reinforcing particles.

nanocomposite specimens. Figure 2 demonstrates the developed apparatus.

A stainless steel mechanical impeller with two 45° flat blades was used to rotate with 2000 rpm in the lower 1/3rd altitude of the melt. Besides, electromagnetic stirring was employed which was made up of a magnetic field with 30 Hz frequency and 5.8 kW. The resultant electromagnetic force made the molten metal rotate in the desired direction with 400 rpm. The sequence of applying the stirring methods could affect the mechanical and metallurgical properties. Hence, different possible sequences were examined separately. Table 1 shows the applied sequences of the stirring methods during first and second steps. As mentioned, electromagnetic stirring usually cannot disperse the nano-sized reinforcements due to its inherent type of stirring, i.e., inducing body force. So, it was not applicable to be used individually as the first step of the stirring process. Also, combination of two stirring methods in the second step (when the temperature is decreasing) is not appropriate due to the high turbulent or velocity.

Hot Extrusion Process

Hot extrusion process was employed, as the secondary bulk forming process, at 350 °C using 20:1 extrusion ratio to reduce porosity and improve mechanical and microstructural properties.^{33,34} The process was implemented using a 100-ton hydraulic press with a ram speed of 5 mm/s. Both machined AZ31B and nanocomposite ingots remained for 1 h at 350 °C to reach steady heat condition. The temperature was monitored precisely at a point close to the extruding region, using a K-type thermocouple. All the mechanical and microstructural tests were done on the hot-extruded samples.

Microstructural and Mechanical Tests

Density of the samples was measured according to Archimedes' principle. The grain sizes in the etched samples were determined during microstructural evaluation using a light optical microscope (LOM). The etchant was composed of 4.2 g picric acid, 10 ml acetic acid, 10 ml distilled water, and 70 ml ethanol. An immersion time of 3–5 s was applied during etching process. Scanning electron microscope (SEM) images helped to observe the microstructures and also the fracture surfaces after the tensile and the high cycle fatigue tests. Particle distribution was observed by a field emission scanning electron microscopy (FE-SEM). Existing precipitation phases in the alloy and the composites were identified by energy-dispersive spectroscopy (EDS) and X-ray diffraction (XRD).

Microhardness tests were implemented by applying 2 N for 10 s as Vickers microhardness method. The microhardness was measured in 10 points of the cross sections

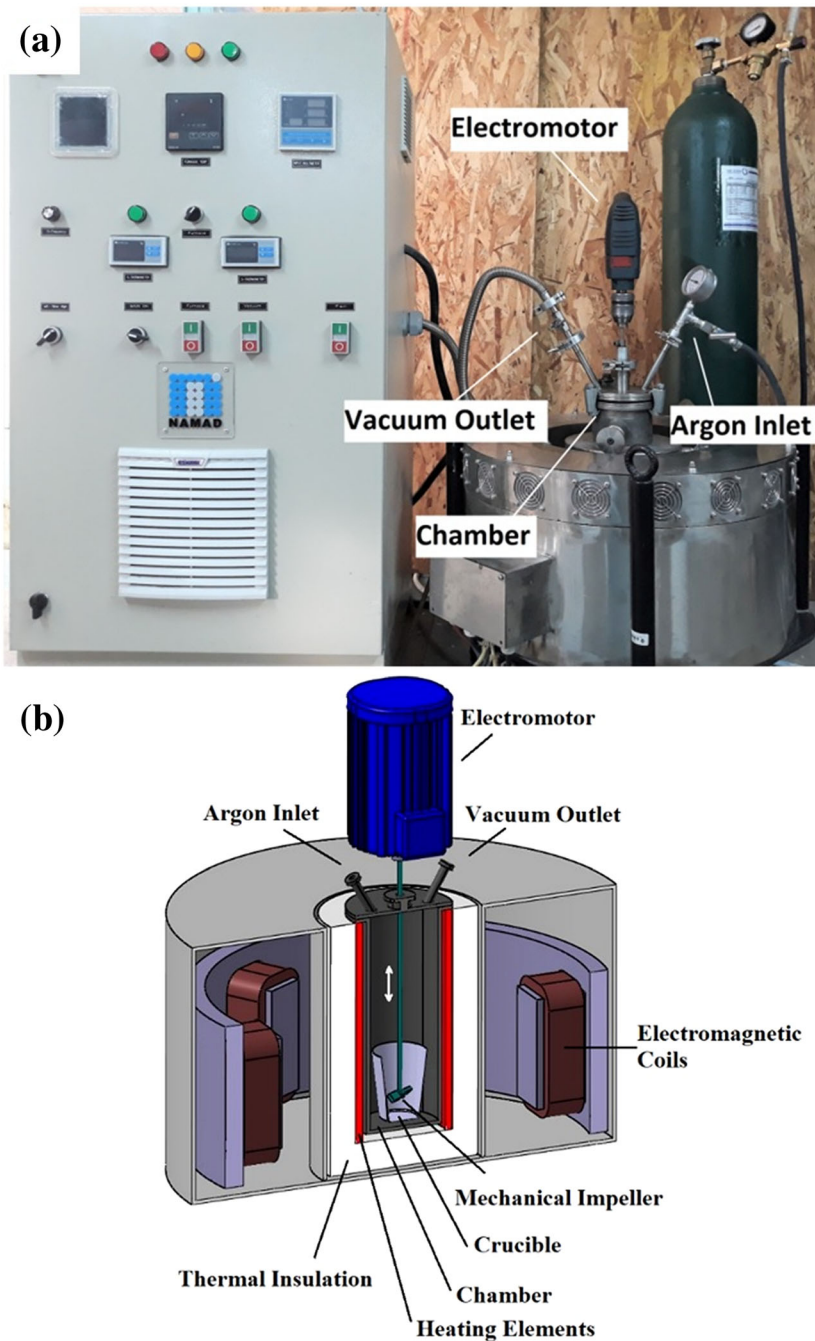


Figure 2. Developed apparatus: (a) different external parts and (b) schematic view of the main parts.

perpendicular to the extrusion direction, and the averaged amounts were reported. The extruded AZ31B and AZ31B/ Al_2O_3 nanocomposites were machined for high cycle fatigue and uniaxial tensile tests.³⁵ Strain rate in the tensile tests was about 0.001 s^{-1} . A rotating bending fatigue test machine with a rotational speed of 6000 rpm and a single-point loading (fully reversed loading, $R = -1$) was utilized. The high cycle fatigue tests were done at room temperature for all the monolithic and the composites samples. The endurance limit of the samples was considered at 10^7 cycles.

Results and Discussions

Density

Experimental density and porosity percentage of the different samples is shown in Figure 3. The results show that Mech–Mech and Combined–Mag–II methods have the most porosity percentages. Indeed, Mech–Mech method did not benefit from electromagnetic stirring step which could let the entrapped gas to float on the melt. In addition, in Combined–Mag–II method, the molten matrix was being

Table 1. Applied Sequences During First and Second Stirring Steps

No.	First stirring step	Second stirring step	Method abbreviated name
1	Mechanical	Mechanical	Mech–Mech
2	Mechanical	Electromagnetic	Mech–Mag
3	Mechanical + electromagnetic (same direction)	Electromagnetic	Combined-Mag-I
4	Mechanical + electromagnetic (inverse direction)	Electromagnetic	Combined-Mag-II

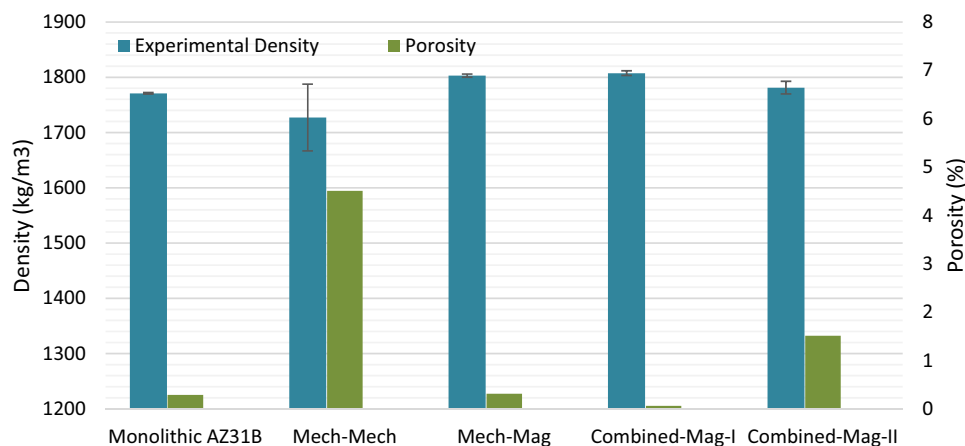


Figure 3. Experimental density and porosity percentage of the different samples.

stirred mechanically and electromagnetically in the inverse directions resulting in more turbulence and gas entrapment. On the other hand, Combined-Mag-I has the less porosity, which could be due to its high stirring speed resulted from same direction stirring.

Microstructure

Figure 4 illustrates the grains morphology in the all-etched samples observed by LOM. It can be seen that all the nanocomposite samples possess finer grains compared to the monolithic AZ31B. This is because of the presence of particulate reinforcement during both solidification and hot extrusion processes.^{30,36} Also, Mech–Mag composite shows the finest grains between composite samples, which could be due to its better particle distribution. A bimodal grain size can be observed in both materials due to the dynamic recrystallization (DRX) phenomenon; however, the composites show less bimodal structure.

Particles in the matrix create many nucleation sites during solidification step which leads to form finer grains.² Also, they restrict the growth of the magnesium grains at higher temperatures as a result of pinning effect,^{36,37} although this effect is not very considerable for nano-sized particles. In addition, extrusion process at elevated temperatures (especially in the presence of reinforcing particles) refines the microstructure by means of DRX.¹⁰ The average grain sizes decreased in the composites by 34.2%, 44.7%, 25.2%,

and 38% for Mech–Mech, Mech–Mag, Combined-Mag-I, and Combined-Mag-II nanocomposites, respectively.

Figure 5 shows the microstructure of the monolithic AZ31B and its composites, using SEM. According to the images, Mech–Mag composite has less and finer second phases when compared to the other composite samples. In addition, in comparison with the monolithic alloy, more secondary phases are observed in the composites as it has been reported previously in the literature.³⁰

Reinforcing particle distribution in the matrix and the presence of different macroscopic and microscopic defects directly influence the resultant mechanical behavior of the produced composites. Indeed, local agglomerations and voids (which could turn into micro-cracks after the extrusion process) are prone areas for crack initiations, continuing as crack propagation and final early failures during loading. Moreover, a uniform distribution of the reinforcements can increase both dislocation density and motion barriers of the dislocations, homogeneously. Figure 6 demonstrates the distribution of the nano-sized particles in the etched composite sample (Mech–Mag) using a FE-SEM.

As it can be observed in Figure 5f, mechanical stirring has resulted in numerous voids in the matrix of the Mech–Mech composite, which could verify the high amount of porosity in this sample (shown in Figure 3). In addition, Combined-Mag-I (Figure 5g) has the most particle

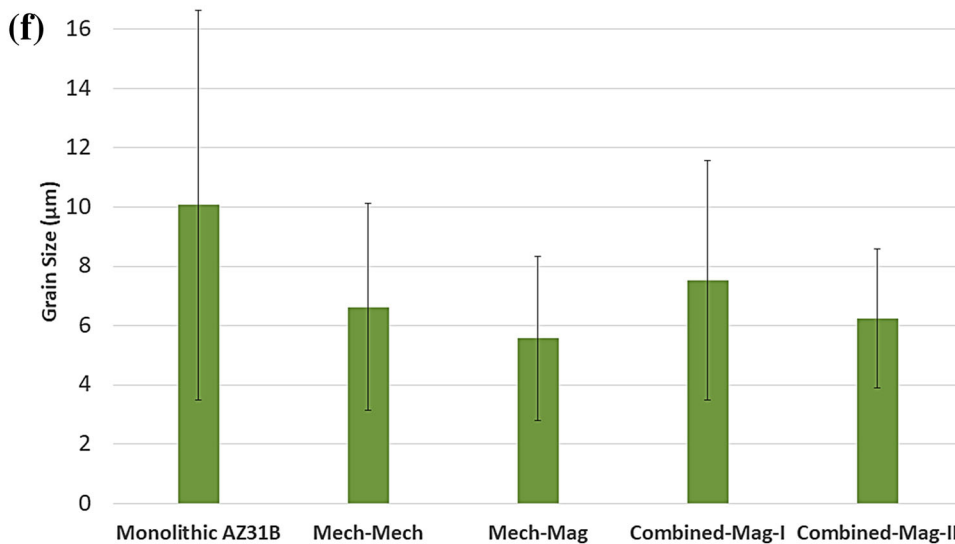
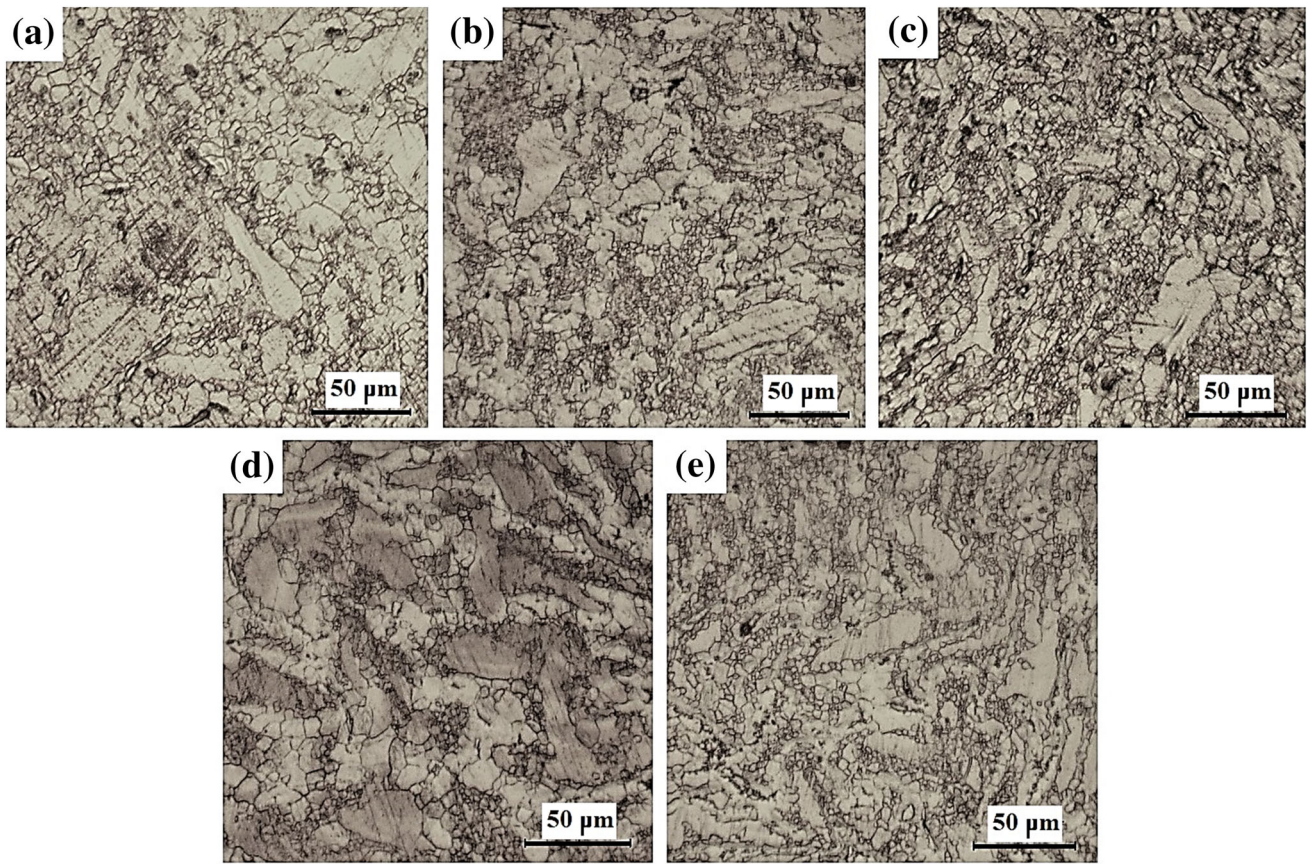


Figure 4. Etched samples show the grains of: (a) AZ31B, (b) Mech–Mech composite, (c) Mech–Mag composite, (d) Combined-Mag-I composite, and (e) Combined-Mag-II composite, and (f) average grain sizes.

agglomerations between different composites, resulting in the least grain refinement and the most heterogeneous microstructure among the composites.

Different secondary phases of the monolithic AZ31B and the composites with their EDS spectrum are demonstrated in Figure 7. According to the EDS results, both AZ31B and

composite samples contain $Mg_{17}Al_{12}$ and $\beta\text{-Mn} + Al_8Mn_5$ phases. Regarding the X-ray diffraction (XRD) results presented in Figure 8, $Mg_{17}Al_{12}$ is the main secondary phase in both alloy and composite samples. It should be noted that other phases were not detected in XRD patterns due to their low volume fractions.

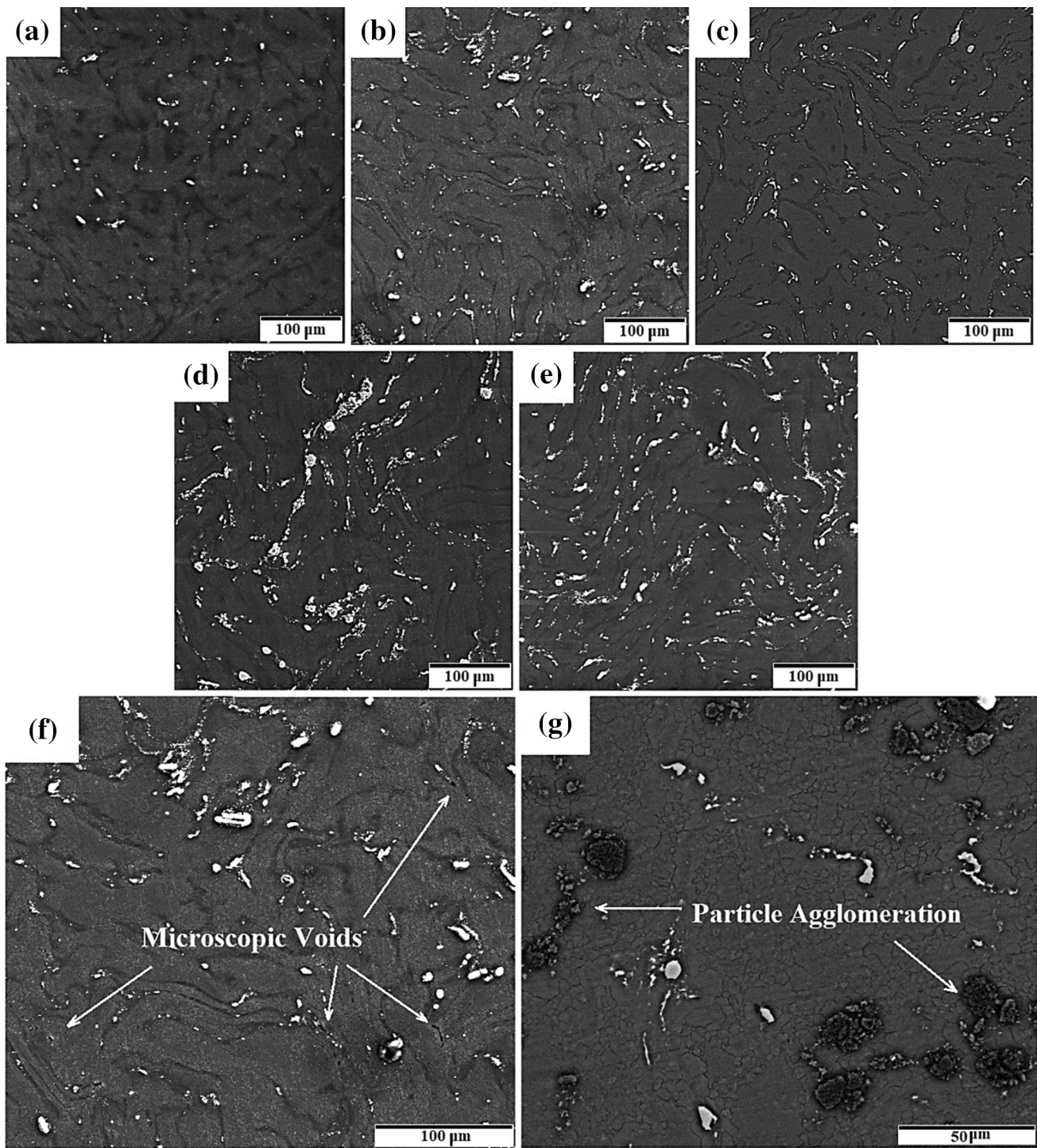


Figure 5. SEM images of the microstructure of: (a) AZ31B, (b) Mech–Mech composite, (c) Mech–Mag composite, (d) Combined–Mag–I composite, (e) Combined–Mag–II composite, and different defects in the composites; (f) microscopic voids in Mech–Mech composite, (g) particle agglomeration in Combined–Mag–I composite.

Vickers Microhardness

Figure 9a shows the results of Vickers microhardness in the monolithic AZ31B and the composite specimens. The microhardness values were increased between 11.6 and 40.8% in all the composite samples in comparison with the alloy. This enhancement was predictable due to the

presence of Al_2O_3 nanoparticles. The nano-sized particles would decrease the grain size, increase the dislocation density, act as barriers for dislocations to restrict or impede their motions, prevent local plastic deformation in the matrix during indentation, and cause Orowan strengthening effect.^{30,38,39} Mech–Mag composite (which has the finest grain size) has the most microhardness improvement,

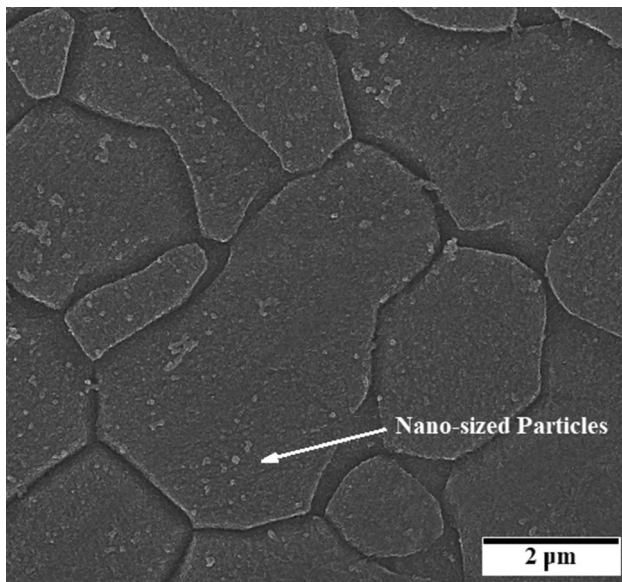


Figure 6. FE-SEM image of the particle distribution in the etched composite sample (Mech-Mag).

where the microhardness was enhanced from 55.2 HV in the AZ31B sample to 77.7 HV in the composite.

Uniaxial Tensile Test

The results of uniaxial tensile tests are shown in Figure 9b. According to the results, the yield stress and ultimate tensile strength (UTS) in the nanocomposites improved compared to the monolithic AZ31B. Generally, overall improvements in the yield stress and the UTS in the MMCs may be ascribed to the interactive effects of the mismatch between elastic modulus and thermal expansion coefficients of the matrix and reinforcing phase (which increases the dislocation density in the matrix), grain refinement (considering Hall-Petch strengthening mechanism⁴⁰), barricading dislocation motions, Orowan strengthening mechanism, and tolerating a part of external far-field loads (which happens using some shear mechanisms in the matrix-reinforcement interfaces).^{41,42} It should be noted that due to little amount of the reinforcement, the increase in the yield stress and UTS is not very considerable.

The results show that Combined-Mag-I composite sample (with less amount of porosity) has the highest amount of tensile yield stress with 10% improvements compared to the monolithic sample. On the other hand, Mech-Mag composite has the highest UTS (12% improvement) and the maximum elongation (16% improvement) in the tensile test.

Compared to the microhardness enhancement, the yield stress and the UTS of the composite samples exhibit less increase. It could be attributed to the detrimental effects of the defects such as micro-cracks, microscopic and

macroscopic voids, and particle agglomerations on the macroscopic tensile behavior, while in the microhardness test a microindenter with a highly localized effect is used.³⁰

Adding a brittle ceramic phase tends to reduce the ductility of the fabricated composites. This may happen, particularly when there are some clusters or agglomerations of the reinforcing particles. Nevertheless, nano-sized particles may increase the ductility by grain refinement (which could improve ductility of metals with hexagonal close-packed structures) and decreasing the size and roundness of the second phases.⁸ Besides, the presence of nano-sized particles during extrusion could assist in the activation of prismatic and cross-slip systems in the matrix, in addition to the basal slip system.²⁹ It should be noted that desirable distribution of nanoparticles and lack of considerable particle clusters are necessary to let these advantages be dominated and decrease the possibility of crack initiation. According to the results, in Combined-Mag-I and Combined-Mag-II samples, the presence of particle agglomerations and porosity could have negative effects. So, the ductility was reduced in these samples. On the other hand, Mech-Mag sample has more ductility compared to the monolithic AZ31B specimen, which could be noted as another reason for existing of a desirable particle distribution in this composite.

High Cycle Fatigue

Figure 10 shows the results of high cycle fatigue (HCF) tests for monolithic AZ31B and the composite samples. The tests were performed at different stress amplitudes. The arrows on the diagram mean that the samples did not fail after 10^7 cycles. The results of stress amplitude versus the number of cycles-to-failure (S-N) curves show that the stirring method strongly affects the HCF behavior of the specimens.

In general, finer grains in the composite could be an advantage to retard the crack initiation resulting in cyclic fatigue life improvement. In addition, reinforcing particles with high elastic modulus and strength could carry a considerable part of the far-field tensile load at the microscopic level. Consequently, the matrix would experience a lower strain in comparison with the AZ31B samples.³⁰ On the other hand, the presence of the voids and agglomerations of the reinforcing phase would act as stress concentration points, resulting in acceleration of crack initiation step. Fatigue cracks initiate at slip bands in defect-free magnesium samples, and the crack initiation stage could be up to 90% of the fatigue life (total of the crack initiation and the crack propagation stages), especially at low stress amplitudes. Nevertheless, high stress concentration in the presence of different defects causes crack initiation, resulting in considerable reduction in the crack initiation stage and decreasing the total fatigue life.²⁴

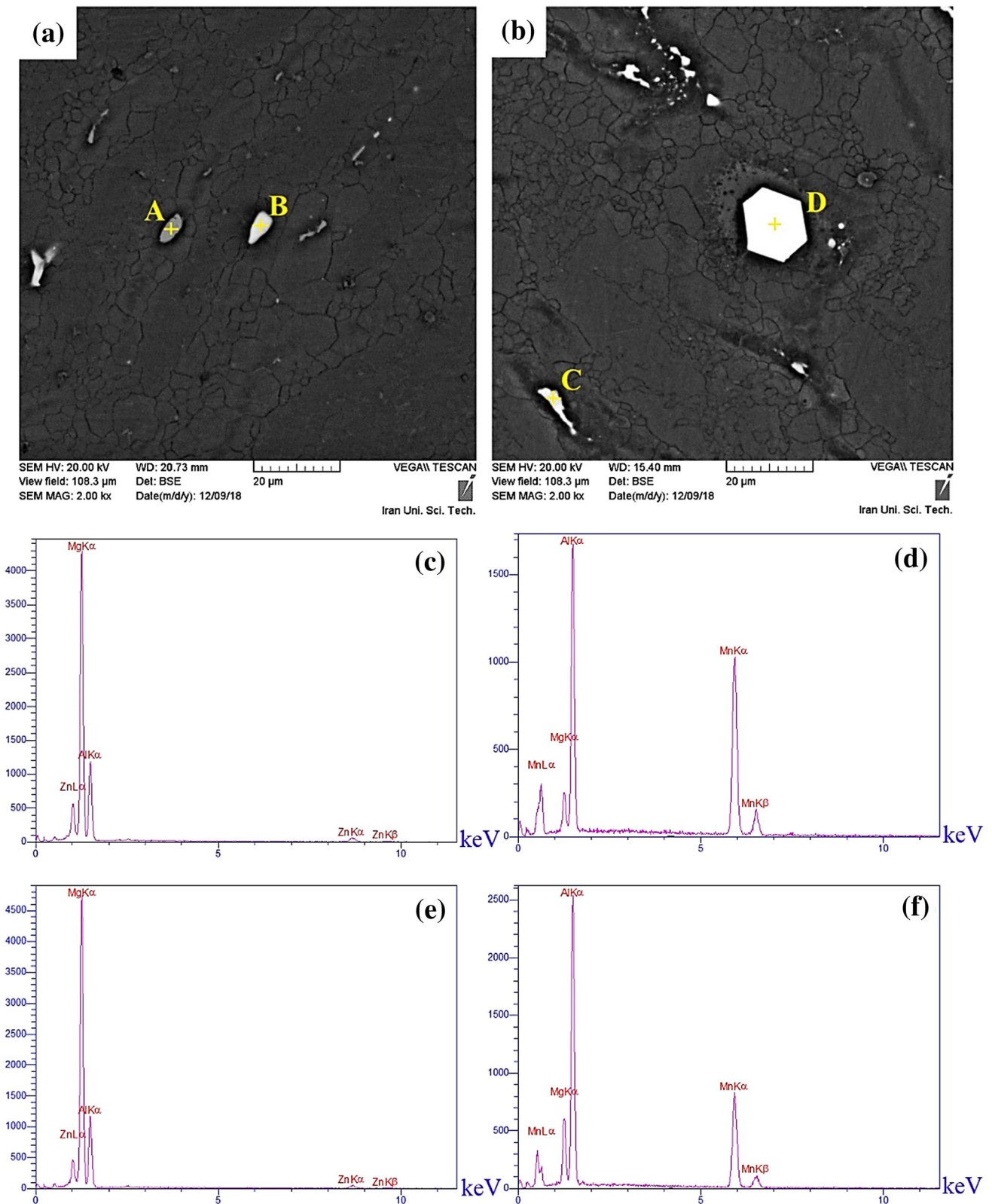


Figure 7. Secondary phases in the samples: (a) AZ31B and (b) composite, and EDS spectrum of different phases in the AZ31B and composite: (c) region A; (d) region B; (e) region C; (f) region D.

For two cases (Mech–Mag samples and Combined-Mag-I), the fabricated composites had an improved HCF behavior compared to the monolithic AZ31B, while fatigue behavior

was degraded in two other cases, Mech–Mech and Combined-Mag-II, which have the most amount of porosity. The most possible reasons of this degradation could be the

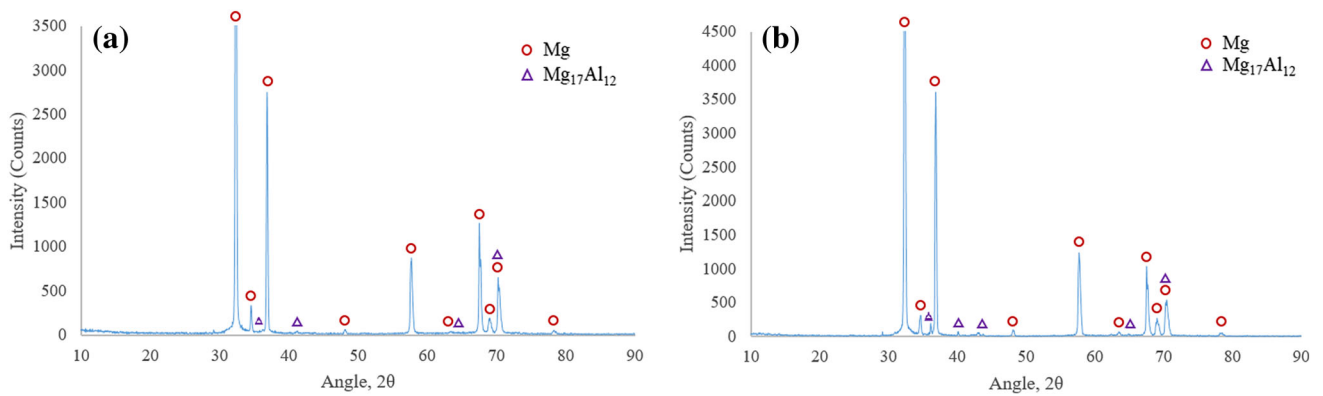


Figure 8. XRD patterns of the samples: (a) AZ31B and (b) composite.

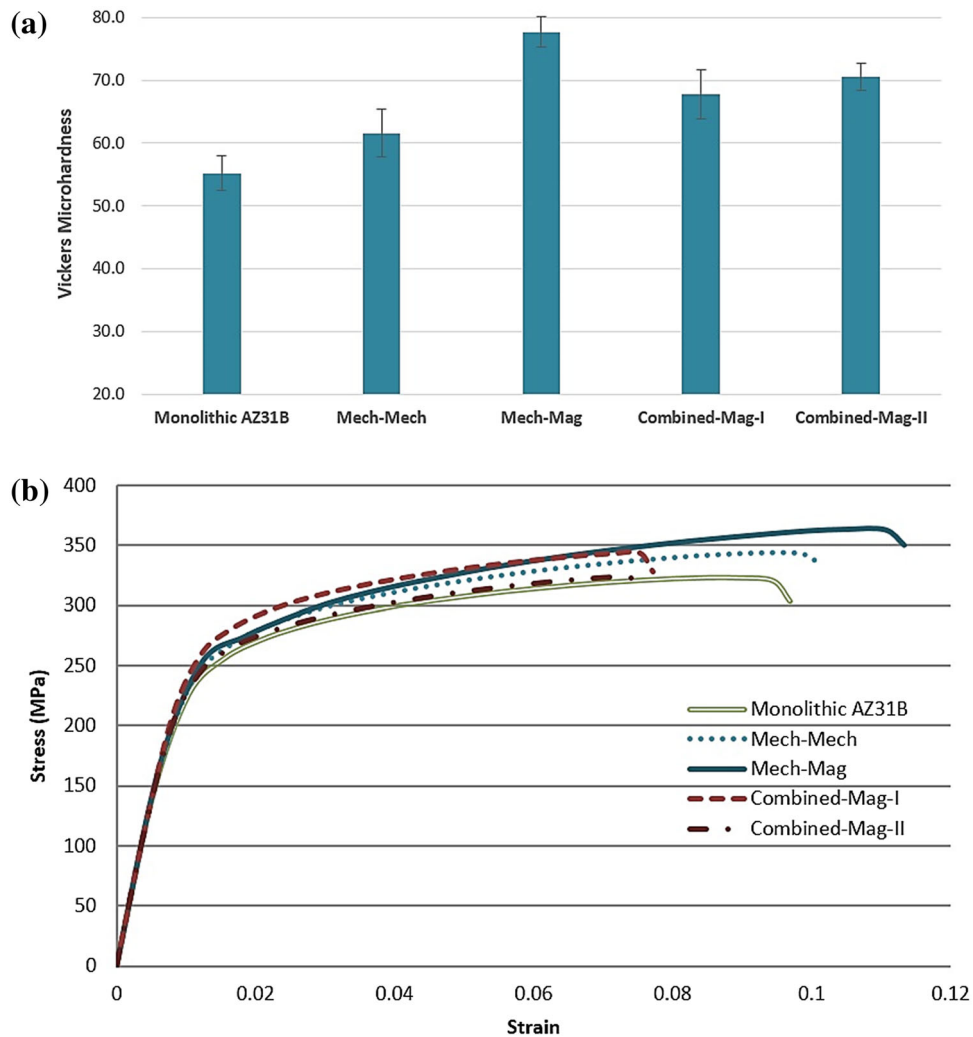


Figure 9. Microhardness and tensile test results of the samples: (a) microhardness and (b) uniaxial tensile test.

more considerable presence of pores (entrapped gas) and also particle agglomerations (poor quality of the particle distribution) in the composites. In the Mech–Mech method, the melt was stirred only mechanically. Hence, there was a little chance for the entrapped gas bubbles and big particle agglomerations to come out of the melt. However,

implementing the electromagnetic stirring offers this opportunity. The results of Mech–Mech samples also show an unreliable behavior. It means that the results do not have a specific trend. It could be due to the presence of more micro-cracks and voids (according to Figure 5f) in the extruded samples. In Combined-Mag-II method, the melt

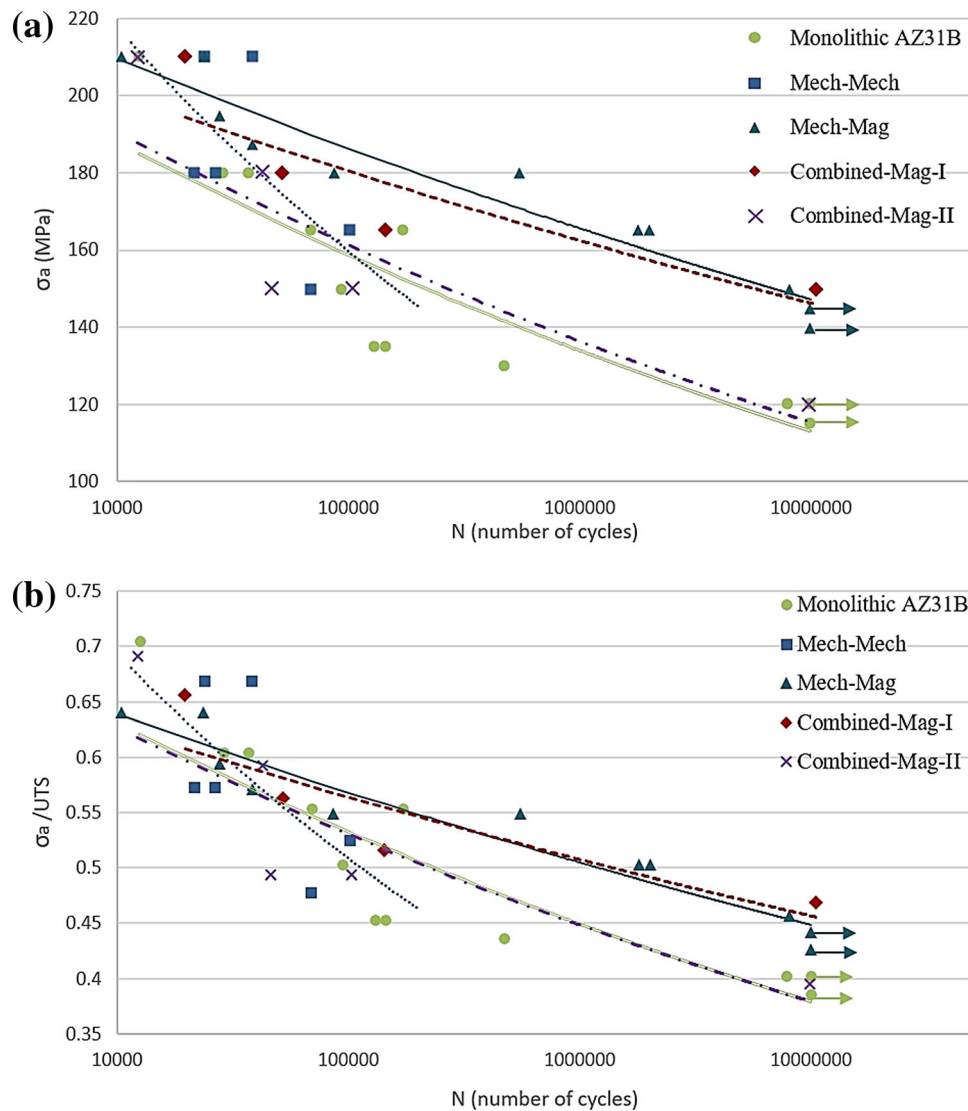


Figure 10. High cycle fatigue results: (a) stress amplitude versus the number of cycles-to-failure (S–N) curves, (b) normalized stress versus the number of cycles-to-failure curves.

was stirred by electromagnetic and mechanical stirring techniques simultaneously in inverse directions at the first step of the stirring. This stirring makes a considerable turbulence in the molten metal resulting in more gas entrapment and porosity. If these defects remain until the end of the stirring process, they could act as crack initiation points.

For Combined-Mag-I (sample with the least amount of porosity), the melt was stirred firstly by electromagnetic and mechanical method in the same directions which results in increasing the total velocity of the melt during stirring. The HCF behavior of this sample has been improved in comparison with the monolithic AZ31B. The most desirable results belong to Mech–Mag composite. It shows that stirring the melt mechanically followed by electromagnetic stirring would cause both better particle distribution and elimination of the trapped gas bubbles and

big agglomerations. In this regard, the endurance limit of the AZ31B sample was improved from 120 to 145 MPa in Mech–Mag composite.

The relation between the applied stress amplitude, σ_a , and the number of cycles to failure, N_f , could be expressed by Basquin's equation as it is shown in Eqn. 1:

$$\sigma_a = \sigma'_f (N_f)^b \quad \text{Eqn. 1}$$

where σ'_f and b are the fatigue strength coefficient and the fatigue strength exponent, respectively. The constants of Basquin's equation for different samples (found by regression analysis using least squares method) are presented in Table 2, where R^2 is R-squared value.

For better comprehension, the normalized stress (σ_a/UTS) versus the number of cycles-to-failure diagram is displayed in Figure 10b. According to the obtained curves, the

Table 2. Basquin's Equation Constants for Different Samples

Sample	σ'_f	b	R^2
(AZ31B)	370.7	- 0.074	0.801
(Mech-Mech)	750	- 0.134	0.4069
(Mech-Mag)	336.2	- 0.051	0.9325
(Combined-Mag-I)	305.7	- 0.046	0.7857
(Combined-Mag-II)	372.8	- 0.073	0.7897

difference between the curves of monolithic AZ31B, Mech-Mag, and Combined-Mag-I is reduced in the normalized diagram. It means that UTS improvement had an important role in the HCF behavior.

Fracture Surface

Fracture surfaces of the monolithic AZ31B and Mech-Mag composite samples (the best composite) resulted from uniaxial tensile test are presented in Figure 11. The fracture surfaces of both monolithic and composite samples

show a mixture of local brittle and ductile behaviors; however, the images demonstrate less microscopic cracks and more dimples in the composite sample, showing more ductile behavior in the composite.

Figure 12 shows the overall morphology of the fracture surfaces in the monolithic AZ31B and Mech-Mag composite samples after HCF tests under different stress amplitudes of 210 MPa and 150 MPa. The surfaces can be divided into two general regions: propagation and sudden fracture (overload) regions. As it was expected, the cracks propagated widely in the tests with low stress amplitudes compared to the high stress amplitude ones. No benchmark pattern can be observed in the macroscopic view of the fracture surfaces.

Crack propagation and sudden fracture regions of the samples are illustrated in Figures 13 and 14 under stress amplitudes of 150 MPa and 210 MPa, respectively. Figure 13a-f and also Figure 14a-f show the crack propagation regions in the monolithic AZ31B and Mech-Mag composite samples. According to the SEM images, the stable crack growth region of the alloy sample shows near featureless transgranular regions with the presence of

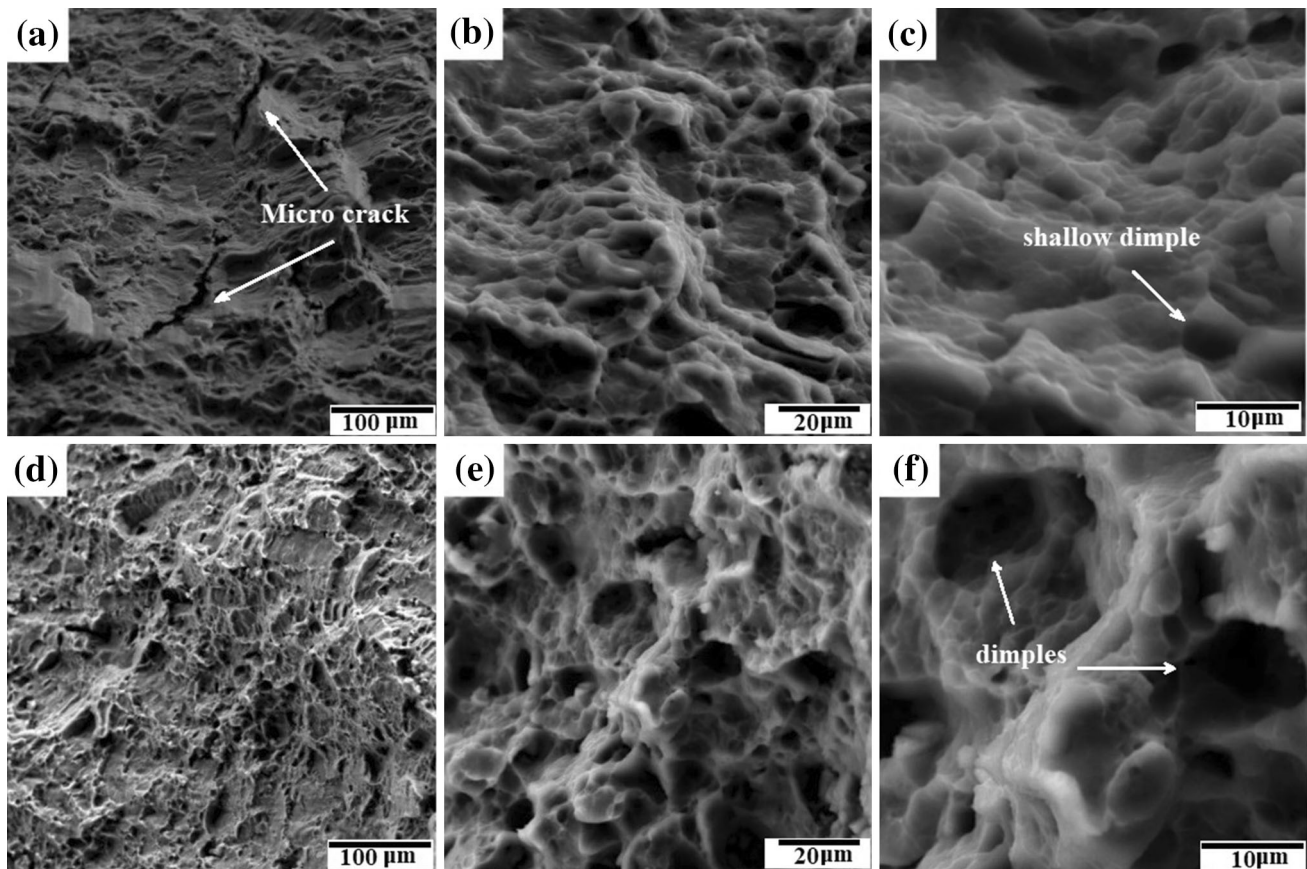


Figure 11. SEM images of tensile tests fracture surfaces of: (a) monolithic AZ31B-500X, (b) monolithic AZ31B-2.00kX, (c) monolithic AZ31B-5.00kX, (d) Mech-Mag composite-500X, (e) Mech-Mag composite-2.00kX, and (f) Mech-Mag composite-5.00kX.

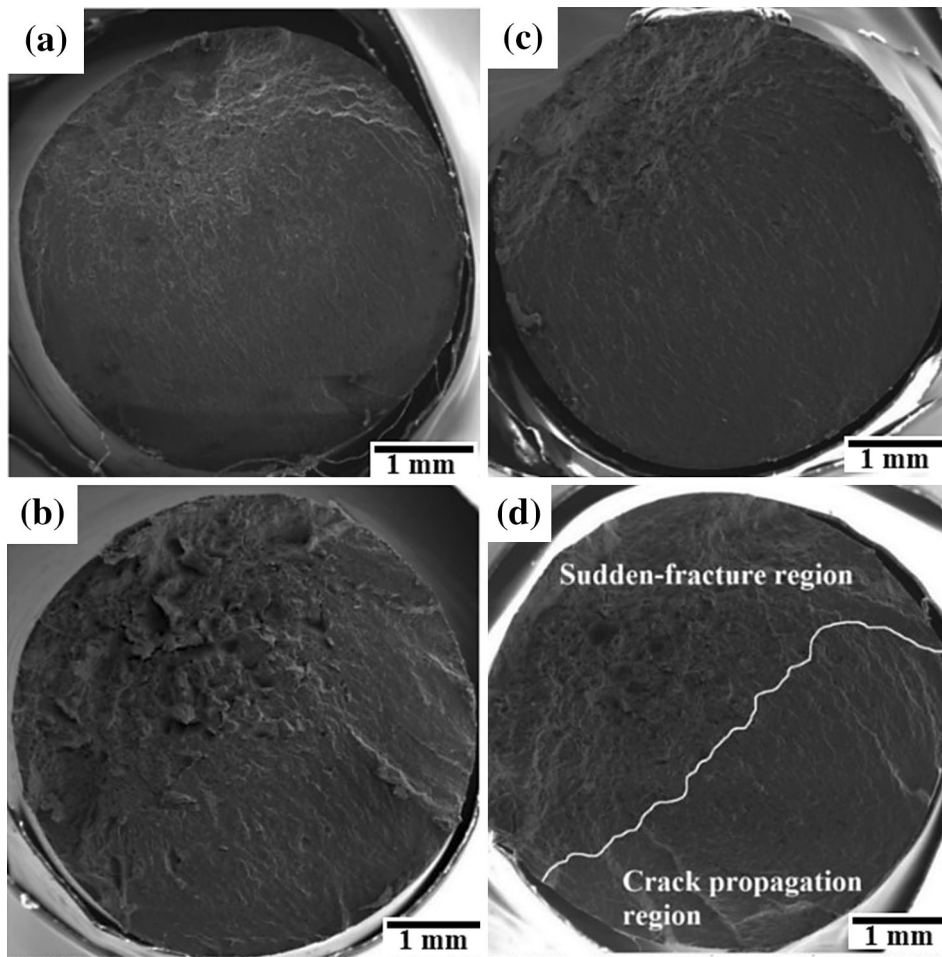


Figure 12. SEM images of the overall morphology of the fractured surfaces in HCF: (a) AZ31B, $\sigma_a = 150$ MPa, (b) AZ31B, $\sigma_a = 210$ MPa, (c) Mech–Mag composite, $\sigma_a = 150$ MPa, and (d) Mech–Mag composite, $\sigma_a = 210$ Mpa.

micro-cracks and tear ridges indicating a brittle failure mechanism. Nevertheless, a random dispersion of shallow dimples and striations packets can be observed in the composite samples as localized micro-plastic deformations.³⁰ Thus, the composite sample shows a more ductile behavior compared to the monolithic alloy. Moreover, the crack propagation region in the composite has a rougher surface. It could be because of finer microstructure and the presence of the nanoparticles, which act as barrier and change the crack propagation path.³⁵ As a result, the crack has to pass a longer path before the final fracture, requiring more cycles to failure.

Parts g and h in Figures 11 and 12 demonstrate sudden fracture region in both monolithic AZ31B and Mech–Mag composite samples. There are numerous microscopic cracks in both samples as an evidence of brittle failure mechanism. Cleavage fracture and delaminated matrix can be observed in the alloy samples. Nonetheless, locally ductile behaviors can be observed in the composite sample due to the presence of dimples and microscopic voids in its

fracture surface. Similarly, such results were observed in the fracture surfaces of the tensile test specimens.

Conclusion

The effects of electromagnetic and mechanical stirring techniques were investigated during fabrication of metal matrix nanocomposites. The conclusions can be summarized as follows:

- The sequence of the mechanical and the electromagnetic stirring could affect the particle distribution and the amount of porosity in the matrix and consequently alter mechanical and microstructural properties. The effect of this sequence was more noticeable on the porosity, tensile, and especially HCF behavior of the composites, although it had considerable effects on the grain size and the microhardness.

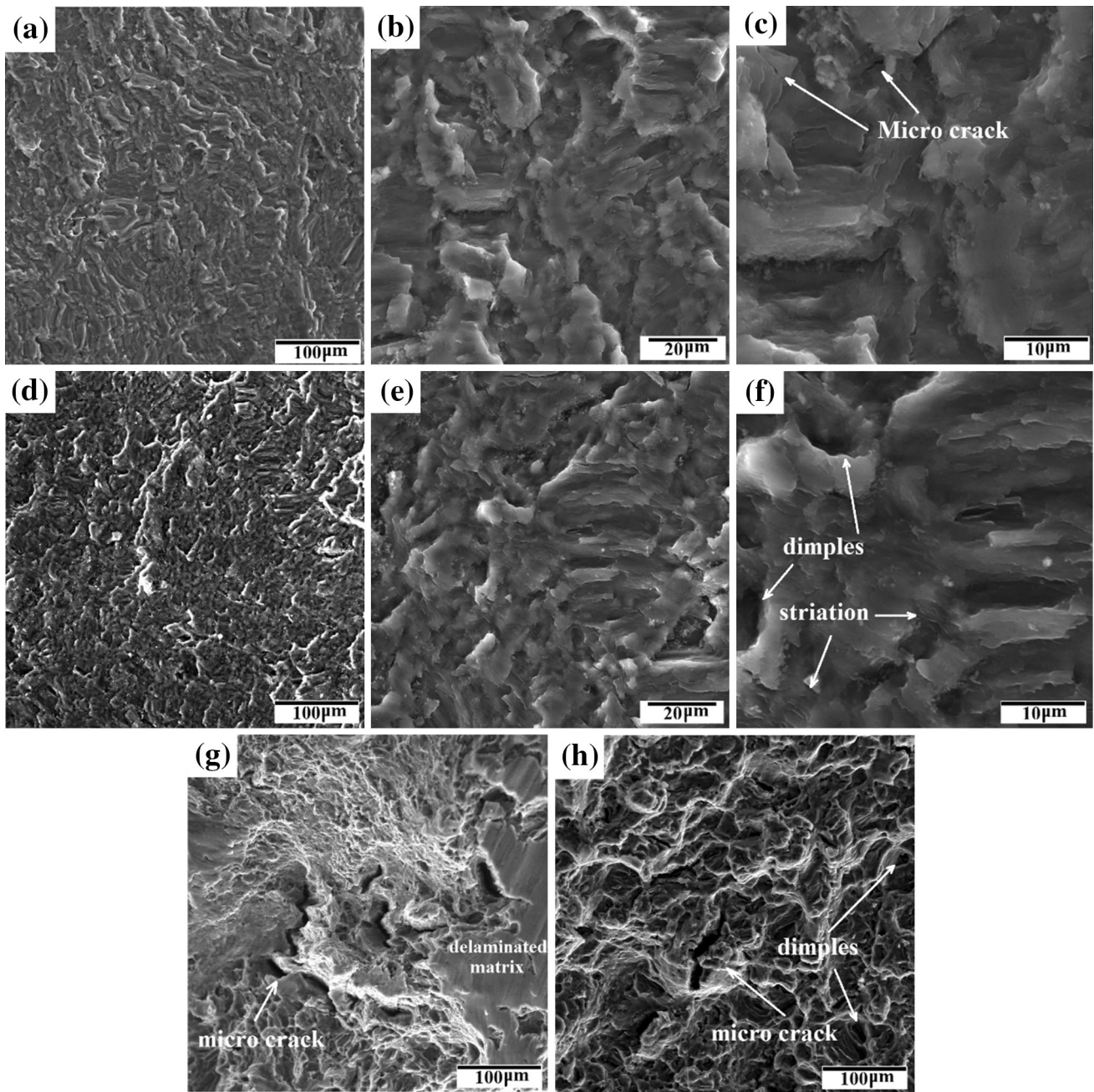


Figure 13. Crack propagation region under $\sigma_a = 150$ MPa: (a) AZ31B-500X, (b) monolithic AZ31B-2.00kX, (c) monolithic AZ31B-5.00kX, (d) Mech-Mag composite-500X, (e) Mech-Mag composite-2.00kX, and (f) Mech-Mag composite-5.00 kX, and sudden fracture region; (g) AZ31B, 500X, and (h) Mech-Mag composite, 500X.

- All the composite samples have finer grains, higher microhardness, and improved tensile properties (yield stress and UTS), compared to the monolithic AZ31B samples.
- The nanocomposite fabricated by mechanical stirring followed by electromagnetic stirring (called Mech-Mag samples), as the best composite, showed about 44.7% reduction in the grain size, 40.8% increase in the microhardness, 12.3% improvement in the UTS, and 16.5% improvement in the maximum elongation, in comparison with the monolithic alloy. Furthermore, in high cycle fatigue regime, the endurance limit of the composite enhanced approximately 21%.
- In Mech-Mag method, after applying the mechanical stirrer, the electromagnetic field stirred the melt using a body force. This body stirring helps to distribute particles better. Additionally, it lets the trapped gas bubbles and considerable particle agglomerations be floated or settled during a separate secondary stirring step. Furthermore, applying electromagnetic stirring during

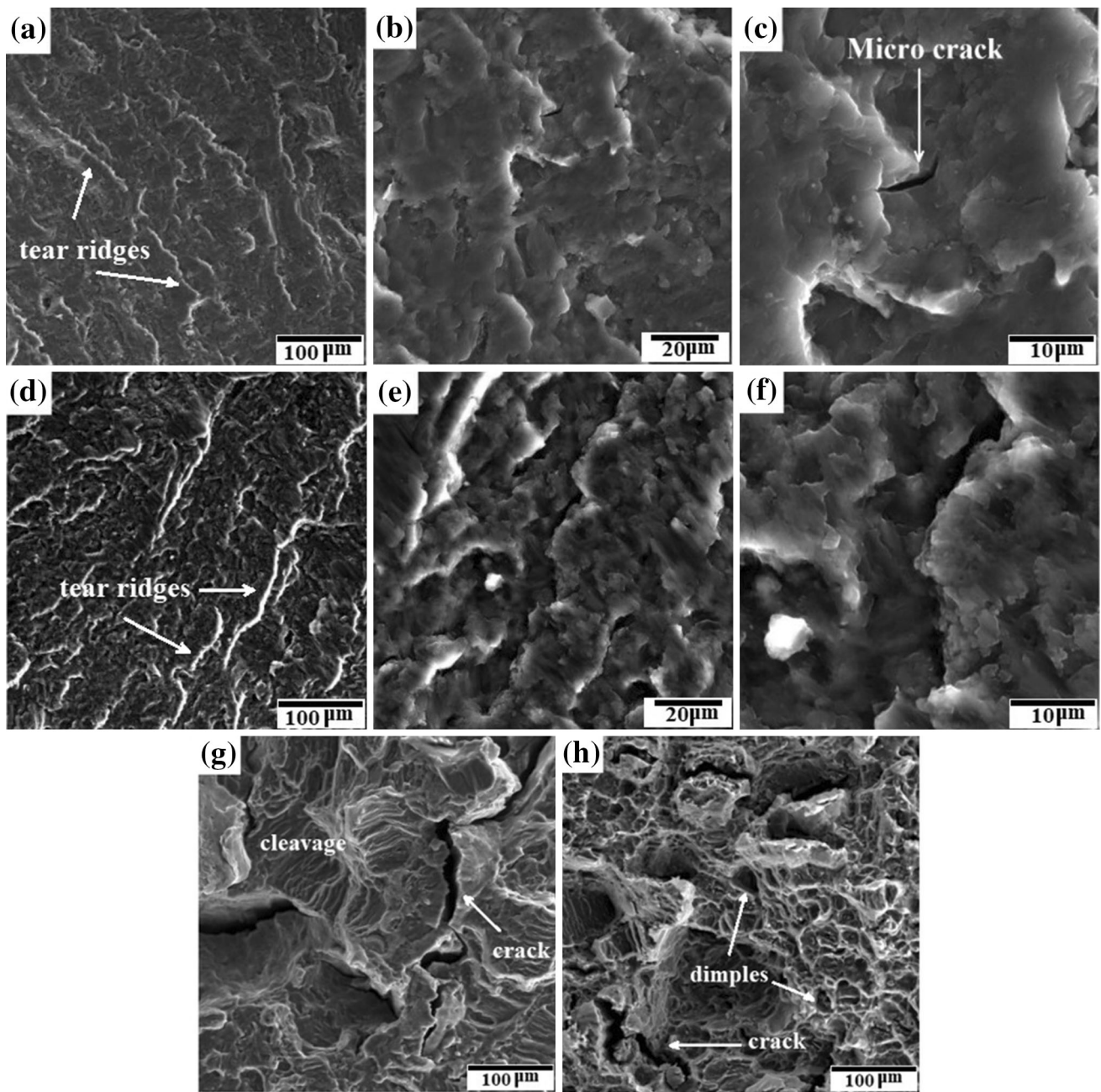


Figure 14. Crack propagation region under $\sigma_a = 210$ MPa: (a) AZ31B-500X, (b) monolithic AZ31B-2.00kX, (c) monolithic AZ31B-5.00kX, (d) Mech-Mag composite-500X, (e) Mech-Mag composite-2.00kX, and (f) Mech-Mag composite-5.00 kX, and sudden fracture region; (g) AZ31B, 500X, and (h) Mech-Mag composite, 500X.

solidification could decrease dendritic structures and grain size, which could reduce undesirable redistribution of the reinforcing particles. Therefore, using mechanical and electromagnetic stirring in a row lessens the defects and porosity in the produced nanocomposite.

- The SEM images of the fracture surfaces showed that the Mech-Mag composite specimens had more ductile behaviors in both tensile and fatigue specimens (in crack propagation and sudden fracture regions). It could be because of

nanoparticle presence, which activates more deformation mechanism in the magnesium matrix of the extruded samples. Also, these particles act as barricade and change the crack propagation path, causing an improvement in HCF behavior of the composite.

Acknowledgements

The authors would like to thank Mr. Arash Shafiee Sabet for his kind help during the experiments.

REFERENCES

1. Q. Chen, G. Chen, L. Han et al., *J. Alloys Compd.* **656**, 67 (2016)
2. M. Habibnejad-Korayem, R. Mahmudi, W. Poole, *Mater. Sci. Eng. A* **519**, 198 (2009)
3. S. Song, X. Zhou, L. Li et al., *Ultrason. Sonochem.* **24**, 43 (2015)
4. A. Azad, L. Bichler, A. Elsayed, *Inter Metalcast* **7**, 49 (2013)
5. X. Zhang, L. Liao, N. Ma et al., *Compos. A* **37**, 2011 (2006)
6. D. Ren, K. Zhao, M. Pan et al., *Scripta Mater.* **126**, 58 (2017)
7. J.E. Sun, M. Chen, G. Cao et al., *J. Compos. Mater.* **48**, 825 (2014)
8. Q. Nguyen, M. Gupta, *J. Alloys Compd.* **459**, 244 (2008)
9. C. Jun, Z. Qing, L. Quanan, *Inter Metalcast* **12**, 897 (2018)
10. Y. Radi, R. Mahmudi, *Mater. Sci. Eng. A* **527**, 2764 (2010)
11. T. Zhong, K. Rao, Y. Prasad et al., *Mater. Sci. Eng. A* **589**, 41 (2014)
12. K. Nie, K. Deng, F. Xu et al., *Mater. Chem. Phys.* **149**, 21 (2015)
13. W.J. Joost, P.E. Krajewski, *Scripta Mater.* **128**, 107 (2017)
14. X. Wang, K. Wu, W. Huang et al., *Compos. Sci. Technol.* **67**, 2253 (2007)
15. M.-J. Shen, T. Ying, F.-Y. Chen et al., *Inter Metalcast* **11**, 287 (2017)
16. M. Paramsothy, X. Tan, J. Chan et al., *J. Alloys Compd.* **545**, 12 (2012)
17. H.Z. Ye, X.Y. Liu, *J. Mater. Sci.* **39**, 6153 (2004)
18. U. Aybarc, H. Yavuz, D. Dispinar et al., *Inter Metalcast* **13**, 190 (2019)
19. I. Ibrahim, F. Mohamed, E. Lavernia, *J. Mater. Sci.* **26**, 1137 (1991)
20. H. Kumar, G. Chaudhari, *Mater. Sci. Eng. A* **607**, 435 (2014)
21. K. Deng, K. Wu, X. Wang et al., *Mater. Sci. Eng. A* **527**, 1630 (2010)
22. S.P. Dwivedi, S. Sharma, R.K. Mishra, *Inter. J. Adv. Res. Innov.* **2**, 639 (2014)
23. A. Kumar, S. Lal, S.J. Kumar, *Mater. Res. Technol.* **2**, 250 (2013)
24. C. Potzies, K.U. Kainer, *Adv. Eng. Mater.* **6**, 281 (2004)
25. J. Hashim, L. Looney, M. Hashmi, *J. Mater. Process. Technol.* **92**, 1 (1999)
26. J. Garcia-Hinojosa, M. Surrapa, *Mater. Sci. Eng. A* **386**, 54 (2004)
27. A.R. Vaidya, J.J. Lewandowski, *Mater. Sci. Eng. A* **220**, 85 (1996)
28. C. Goh, M. Gupta, J. Wei et al., *J. Compos. Mater.* **42**, 2039 (2008)
29. C. Goh, J. Wei, L. Lee et al., *Compos. Sci. Technol.* **68**, 1432 (2008)
30. T. Srivatsan, C. Godbole, T. Quick et al., *J. Mater. Eng. Perform.* **22**, 439 (2013)
31. H.A. Hassan, J.J. Lewandowski, *Mater. Sci. Eng. A* **600**, 188 (2014)
32. X. Liu, S. Jia, L. Nastac, *Inter Metalcast* **8**, 51 (2014)
33. N. Chawla, K.K. Chawla, *Metal Matrix Composites*, 2nd edn. (Springer, New York, 2013)
34. T. Clyne, P. Withers, *An Introduction to Metal Matrix Composites* (Cambridge University Press, Cambridge, 1995)
35. A. Sabet, A. Jabbari, M. Sedighi, *J. Compos. Mater.* **52**, 1711 (2018)
36. A.K. Khanra, H.C. Jung, S.H. Yu et al., *Bull. Mater. Sci.* **33**, 43 (2010)
37. Q. Chen, G. Chen, F. Han et al., *Metall. Mater. Trans. A* **48**, 3497 (2017)
38. A. Singh, N. Bala, *Metall. Mater. Trans. A* **48**, 5031 (2017)
39. S. Hassan, M. Gupta, *Mater. Sci. Eng. A* **425**, 22 (2006)
40. M. Shen, M. Zhang, W. Ying, *J. Magn. Alloys* **3**, 162 (2015)
41. S. Mohammadi, A. Jabbari, M. Sedighi, *J. Mater. Eng. Perform.* **26**, 3410 (2017)
42. E. Suneesh, M. Sivapragash, *Mater. Manuf. Process.* **33**, 1324 (2018)

Publisher's Note Springer Nature remains neutral with regard to jurisdictional claims in published maps and institutional affiliations.